Article

Discovery Medicine 2026; 38(211): 2535–2547
https://doi.org/10.24976/Discov.Med.202638211.200

Structure-Based Identification of HFS764 as an Inhibitor of the HIF-1α–p300 Interface in Hypoxic Renal Cell Carcinoma

Mesfer Mohammad Al Shahrani[1,*]

[1]Department of Clinical Laboratory Sciences, College of Applied Medical Sciences, King Khalid University, 61421 Abha, Saudi Arabia
*Correspondence: mesferm@kku.edu.sa (Mesfer Mohammad Al Shahrani)
Submitted: 27 February 2026 Revised: 23 May 2026 Accepted: 10 June 2026 Published: 24 August 2026

Background: Hypoxia-inducible factor-1 alpha (HIF-1α) drives tumor adaptation to hypoxia by promoting angiogenesis, metabolic reprogramming, and survival signaling in clear cell renal cell carcinoma (ccRCC). Transcriptional activity of HIF-1α depends on its interaction with the p300/CBP (CREB-binding protein) coactivator via the C-terminal transactivation domain (C-TAD). Direct targeting of this protein–protein interface remains limited, highlighting the need for novel inhibitors.
Methods: A structure-based virtual screening of ~250,000 compounds from the ZINC database was conducted to identify candidates targeting a predicted pocket within the HIF-1α C-TAD. Top hits were evaluated using molecular docking and 100 ns molecular dynamics simulations. The lead compound, HFS764, was further characterized using *in silico* absorption, distribution, metabolism, excretion, and toxicity (ADMET) profiling, homogeneous time-resolved fluorescence (HTRF) assays, and differential scanning fluorimetry (DSF). Functional effects were assessed in Caki-1 cells under hypoxia using hypoxia response element (HRE)-luciferase assays, cell viability and vascular endothelial growth factor (VEGF) secretion.
Results: HFS764 demonstrated stable binding within the HIF-1α pocket, with ligand root-mean-square deviation (RMSD) <0.20 nm and a predicted binding free energy of –22.38 kcal/mol. HTRF assays confirmed inhibition of the HIF-1α–p300 interaction (IC_{50} = 4.89 μM), while DSF showed ligand-induced stabilization (ΔT_m = +2.0 °C). In Caki-1 cells, HFS764 suppressed HRE-driven transcription (IC_{50} = 4.27 μM), and reduced VEGF secretion under hypoxia. Selective cytotoxicity was observed (GI_{50}: 14.70 μM in Caki-1 vs. 37.98 μM in HK-2; therapeutic index = 2.58).
Conclusion: HFS764 disrupts the HIF-1α–p300 interface and suppresses hypoxia-driven signaling in ccRCC, supporting the use of transcriptional complex inhibition as a promising therapeutic strategy.

Keywords: hypoxia-inducible factor-1 alpha; p300 coactivator; renal cell carcinoma; hypoxic signaling; angiogenesis; small-molecule inhibitor; transcriptional regulation

Introduction

Renal cell carcinoma (RCC) represents the most common malignancy of the adult kidney, with clear cell renal cell carcinoma (ccRCC) accounting for approximately 70–80% of cases [1]. Despite significant advances in targeted therapies and immune checkpoint inhibitors, advanced ccRCC remains therapeutically challenging. Disease progression is closely associated with metabolic reprogramming, persistent hypoxia, and the emergence of resistance to systemic therapies [2]. A defining molecular hallmark of ccRCC is disruption of oxygen-sensing mechanisms, most frequently due to loss or inactivation of the von Hippel–Lindau (VHL) tumor suppressor gene, leading to stabilization of hypoxia-inducible factor-1 alpha (HIF-1α).

Under normoxic conditions, HIF-1α undergoes prolyl hydroxylation and subsequent proteasomal degradation through the VHL-dependent ubiquitination pathway. In contrast, hypoxia or VHL deficiency prevents hydroxylation, resulting in HIF-1α stabilization, nuclear translocation, and transcriptional activation of genes regulating angiogenesis, glycolysis, glucose transport, and cell survival. Through induction of adaptive gene networks, HIF-1α enables tumor cells to sustain angiogenic signaling and metabolic flexibility under oxygen-limited conditions, positioning it as a central effector of hypoxia-driven tumor biology. Notably, hyperglycemic or high-glucose environments further potentiate HIF-1α activity by enhancing glycolytic flux and oxidative stress, thereby reinforcing a metabolically permissive microenvironment that promotes tumor progression and therapeutic resistance [3,4].

Beyond its role in metabolic adaptation, HIF-1α integrates oncogenic signaling pathways with microenvironmental cues. Activation of HIF-1α influences inflammatory mediators, extracellular matrix remodeling, and immune cell modulation, collectively contributing to tumor invasion, immune evasion, and resistance to therapy [5,6].

Accumulating evidence suggests that HIF-1α functions not merely as a downstream mediator of hypoxic stress but as a dominant transcriptional regulator orchestrating the adaptive tumor response [7,8]. Consequently, therapeutic strategies aimed at directly targeting HIF-1α–dependent transcriptional machinery may provide broader and more durable antitumor effects than approaches limited to downstream angiogenic inhibition.

A critical determinant of HIF-1α transcriptional activity is its interaction with the transcriptional coactivators p300/CBP (CREB-binding protein) through the C-terminal transactivation domain (C-TAD) [9]. Recruitment of p300/CBP is essential for chromatin remodeling and assembly of the transcriptional machinery, enabling efficient activation of hypoxia-responsive genes, including those involved in angiogenesis, glycolysis, and cell survival. Disruption of this coactivator engagement effectively attenuates HIF-1–dependent transcription at its source, offering a mechanistically targeted approach that operates upstream of downstream effector pathways. Despite this therapeutic rationale, direct pharmacological targeting of the HIF-1α–p300 interface remains challenging due to the relatively shallow and dynamic nature of protein–protein interaction surfaces, as well as the intrinsic conformational flexibility of the HIF-1α C-TAD [10]. Existing inhibitors largely act indirectly on HIF signaling or exhibit limited specificity toward this interface, underscoring the need for novel small molecules capable of selectively disrupting the HIF-1α–p300 transcriptional complex.

Given the pivotal role of HIF-1α in hypoxic and metabolic reprogramming, direct disruption of its interaction with transcriptional coactivators such as p300/CBP represents a rational and mechanistically precise therapeutic strategy. Interfering with the HIF-1α–p300 interface may suppress transcriptional activation of hypoxia-responsive genes at its source, thereby attenuating angiogenic and survival signaling programs. In the present study, we employed a structure-based computational screening approach combined with biochemical and cellular validation to identify and characterize novel inhibitors of the HIF-1α transcriptional complex under hypoxic conditions. By selectively targeting the hypoxia-driven transcriptional program rather than secondary metabolic consequences, this strategy aims to impair tumor adaptation and enhance therapeutic susceptibility in hypoxia-dependent RCC.

Materials and Methods

Protein Structure Preparation

The three-dimensional structure of human HIF-1α (UniProt ID: Q16665) was retrieved from the AlphaFold Protein Structure Database. Prior to computational analyses, the structural model was refined to ensure suitability for molecular docking studies. Regions with low confidence scores or predicted intrinsic disorder were excluded to enhance structural reliability, and residues 1–352 corresponding to the structured domain were retained for subsequent analysis. The processed structure was prepared using molecular modeling software, including structural optimization and side-chain refinement. Potential ligand-binding sites were identified using cavity detection algorithms to delineate druggable pockets within the HIF-1α structure.

High-Throughput Virtual Screening

A diversity-oriented high-throughput virtual screening campaign was conducted using a natural product-like subset of the ZINC database comprising approximately 250,000 small molecules. Molecular docking was performed using AutoDock Vina with an exhaustiveness value of 8 and generation of up to 10 binding poses per ligand. The docking grid was centered on the predicted cavity within HIF-1α and defined with dimensions of 20 × 20 × 20 Å. Compounds were ranked according to predicted binding free energy, and the top-ranked poses were visually inspected for consistency of binding orientation and interaction with residues lining the predicted pocket. Top-performing compounds demonstrating favorable binding profiles were selected for subsequent structural and experimental validation.

Molecular Dynamics Simulation

To assess the dynamic stability of the HIF-1α–HFS764 complex, molecular dynamics (MD) simulations were performed using GROMACS version 2021 through the SiBioLEAD standalone graphical interface for computer-aided drug discovery on an Ubuntu 24.04 workstation equipped with an NVIDIA graphics processing unit. The protein–ligand complex was prepared using the integrated preprocessing module. The system was solvated in a triclinic simulation box containing Simple Point Charge (SPC) water molecules with a minimum distance of 1.0 nm between the complex and the box boundaries.

The OPLS force field was applied for system parameterization. Appropriate sodium and chloride ions were added to neutralize the system and achieve a physiological ionic strength of 0.15 M. Energy minimization was performed using the steepest descent algorithm until convergence to eliminate unfavorable steric contacts.

Following minimization, the system underwent equilibration in two phases: constant volume and temperature (NVT) equilibration at 300 K, followed by constant pressure and temperature (NPT) equilibration at 1 bar for a total duration of 300 ps. Temperature and pressure were maintained using standard coupling algorithms implemented in GROMACS.

Long-range electrostatic interactions were calculated using the Particle Mesh Ewald method, and van der Waals interactions were treated using a cutoff of 1.0 nm. All covalent bonds involving hydrogen atoms were constrained

using the LINCS algorithm, allowing an integration time step of 2 fs. Neighbor lists were updated every 10 steps. Temperature was maintained at 300 K using the V-rescale thermostat, and pressure was maintained at 1 bar using the Parrinello–Rahman barostat. Trajectory coordinates were saved every 10 ps for subsequent analysis. A 100 ns production MD simulation was subsequently carried out under periodic boundary conditions. Structural stability of the complex was evaluated by calculating the root-mean-square deviation (RMSD) of backbone atoms over time. Protein–ligand interaction stability was further assessed by monitoring hydrogen bond occupancy, hydrophobic contacts, and interaction persistence throughout the simulation trajectory. Post-simulation analyses included backbone and ligand RMSD, hydrogen bond occupancy, and visual inspection of initial and final binding poses. Binding free energy calculations were performed using the MM/PBSA method on equilibrated trajectory frames, and energy components (van der Waals and electrostatic) were extracted accordingly. Representative structural snapshots were selected from the stabilized phase of the trajectory based on RMSD convergence. Structural visualization and trajectory analyses were performed using the SiBioLEAD graphical interface and Discovery Studio Visualizer.

ADMET Prediction

The pharmacokinetic and toxicity profiles of the selected compounds were evaluated using an in silico absorption, distribution, metabolism, excretion, and toxicity (ADMET) prediction platform. Key parameters related to intestinal absorption, blood–brain barrier permeability, metabolic stability, cytochrome P450 interactions, clearance, and predicted toxicity endpoints were assessed to estimate drug-likeness and safety profiles. Predictions were generated using the ADMET-AI web server [11].

HTRF Assay for HIF-1α–p300 Interaction

The inhibitory activity of HFS764 (N-cycloheptyl-9-oxo-1H,2H,3H,9H-pyrrolo[2,1-b]quinazoline-6-carboxamide; ZINC ID: ZINC15658755; MolPort ID: Molport-008-347-413, MolPort, Riga, Latvia) on the HIF-1α–p300 interaction was evaluated using a homogeneous time-resolved fluorescence (HTRF) assay. Experiments were conducted using the HTRF Human and Mouse HIF-1α Detection Kit (Cisbio Bioassays, Revvity France; Cat. No. 64HIFPEG), which employs a time-resolved fluorescence resonance energy transfer donor/acceptor antibody pair to quantify HIF-1α binding in a cell-free format.

Stock solutions of HFS764 and the reference inhibitor YC-1 (Sigma-Aldrich, St Louis, MO, USA; Cat. No. Y102) were prepared at 10 mM in dimethyl sulfoxide. All assay reagents were equilibrated to room temperature prior to use. Reactions were assembled in low-volume white 384-well plates (Corning Costar, Tewksbury, MA, USA; Cat. No. 4512) in a total volume of 10 µL using the HTRF detection buffer provided in the kit. HFS764 was tested in an eight-point half-log serial dilution ranging from 0.01 to 50 µM, with the final dimethyl sulfoxide concentration maintained at 1% (v/v) in all wells.

Each reaction mixture contained the recommended concentrations of biotinylated HIF-1α peptide, antibody pairs, and detection reagents supplied by the manufacturer. Vehicle control (1% dimethyl sulfoxide), an unlabeled competitor peptide provided in the kit, and YC-1 (30 µM) were included as controls. Plates were sealed and incubated for 30–60 min at room temperature protected from light. The concentration range for HFS764 (0.01–50 µM) was selected based on preliminary dose–response experiments to capture the full dynamic range of inhibition. YC-1 was evaluated over a similar µM range to enable direct comparison and is consistent with previously reported concentrations used in HIF-1α inhibition assays [12].

Time-resolved fluorescence signals were measured using a BMG Labtech FLUOstar Omega (Ortenberg, Germany) plate reader with excitation at 337 nm and dual-emission detection at 620 nm (donor) and 665 nm (acceptor). Data were expressed as the 665/620 nm emission ratio multiplied by 10,000. Percent inhibition was calculated relative to vehicle-treated controls. Concentration–response curves were fitted using a four-parameter logistic model in GraphPad Prism (version 6.0; GraphPad Software Inc., San Diego, CA, USA) and half maximal inhibitory concentration values were derived from three independent experiments performed in technical triplicate.

YC-1 was included as a reference HIF pathway inhibitor. Although YC-1 does not directly disrupt the HIF-1α–p300 protein–protein interaction, it has been widely used as a functional inhibitor of HIF-1α activity and was therefore employed as a comparator to benchmark assay performance.

Differential Scanning Fluorimetry

Differential scanning fluorimetry (DSF) was performed to assess direct binding of HFS764 to the HIF-1α C-terminal transactivation domain (C-TAD). Recombinant HIF-1α C-TAD (residues 776–826; Cat. No. SRP2097, Sigma-Aldrich, St Louis, MO, USA) was prepared at a final concentration of 2–4 µM in DSF buffer consisting of 20 mM HEPES (pH 7.4), 150 mM sodium chloride, and 2 mM dithiothreitol. SYPRO Orange dye (Thermo Fisher Scientific, Eugene, OR, USA, Cat. No. S6650) was freshly diluted 1:1000 in assay buffer immediately before use.

HFS764 and the reference inhibitor YC-1 were diluted from 10 mM dimethyl sulfoxide stock solutions into assay buffer to achieve a final concentration of 50 µM, with the dimethyl sulfoxide concentration maintained at 1% (v/v) in all experimental conditions. Vehicle controls contained 1% dimethyl sulfoxide without compound. Reaction mixtures (20 µL total volume) were assembled in hard-shell 96-well

optical PCR plates (Bio-Rad, Hercules, CA, USA; Cat. No. HSP9601), sealed with optically clear PCR film, and briefly centrifuged to remove air bubbles.

Thermal denaturation profiles were acquired using a Bio-Rad CFX96 Real-Time PCR system (Bio-Rad, Hercules, CA, USA)with a temperature gradient from 25 °C to 95 °C in 0.5 °C increments. Fluorescence was recorded at each temperature step using the instrument channel appropriate for SYPRO Orange detection. Melting temperatures (T_m) were calculated from the peak of the first derivative of the fluorescence curve (–dF/dT) using Bio-Rad CFX Manager software. Thermal shift values (ΔT_m) were determined relative to vehicle-treated controls. Experiments were performed in three independent biological replicates, each conducted in technical triplicate, and data are presented as mean ± standard deviation (SD).

HRE-Luciferase Reporter Assay

HIF-1 transcriptional activity was quantified using a hypoxia response element (HRE)-driven dual-luciferase assay in Caki-1 cells (ATCC, Manassas, VA, USA; Cat. No. HTB-46). Cells were maintained in McCoy's 5A medium (Gibco, Grand Island, NY, USA; Cat. No. 16600-082) supplemented with 10% fetal bovine serum (Gibco, Grand Island, NY, USA; Cat. No. 16000-044) and 1% penicillin–streptomycin (Gibco, Grand Island, NY, USA; Cat. No. 15140-122) at 37 °C in a humidified atmosphere containing 5% carbon dioxide.

Cells were seeded in white opaque 96-well plates (Corning Costar, Tewksbury, MA, USA; Cat. No. 3917) at a density of 1.2×10^4 cells per well and allowed to adhere overnight. Transient co-transfection was carried out using 100 ng per well of a 5×HRE firefly luciferase plasmid (Addgene, Watertown, MA, USA; Cat. No.26731) together with 10 ng per well of the pRL-TK Renilla luciferase control vector (Promega Corporation, Madison, WI, USA; Cat. No. E2241). Transfection complexes were prepared in Opti-MEM reduced serum medium using Lipofectamine 3000 and P3000 reagent (Invitrogen, NY, USA) according to the manufacturer's protocol.

Following a 24-hour post-transfection incubation period, cells were treated with HFS764 at concentrations of 0.01, 1, 3, 10, and 30 µM, prepared in dimethyl sulfoxide with a final solvent concentration of 0.1% (v/v). Vehicle control wells received 0.1% dimethyl sulfoxide. The reference HIF pathway inhibitor YC-1 (Sigma-Aldrich, Cat. No. Y102) was included as a comparator and evaluated across the same concentration range. The selected concentration range was chosen to encompass submaximal to near-saturating inhibitory effects based on preliminary optimization studies. These concentrations are consistent with reported µM activity of YC-1 and related HIF pathway inhibitors in cellular assays [12,13].

To model hypoxic metabolic stress, treatments were conducted in high-glucose Dulbecco's modified Eagle medium (25 mM glucose; Gibco, Grand Island, NY, USA; Cat. No. 11966-025) under controlled hypoxic conditions (1% oxygen, 5% carbon dioxide, balance nitrogen) using a tri-gas incubator (Galaxy 48 R, Eppendorf, Enfield, CT, USA). Normoxic controls (21% oxygen) were maintained in standard glucose medium (5.5 mM glucose). After 18 hours of hypoxic exposure, luciferase activity was determined using the Dual-Luciferase Reporter Assay System (Promega Corporation Madison, WI, USA; Cat. No. E1910) in accordance with the manufacturer's instructions. Luminescence was measured using a FLUOstar Omega microplate reader (BMG Labtech, Ortenberg, Germany). Firefly luciferase activity was normalized to Renilla luciferase activity to correct for transfection efficiency. Percent inhibition was calculated relative to hypoxia plus vehicle-treated controls.

All cell lines used in this study were authenticated by short tandem repeat (STR) profiling and were confirmed to be free of mycoplasma contamination prior to experimentation. All experiments were performed in three independent biological replicates, each conducted in technical triplicate. Concentration–response curves were fitted using a four-parameter logistic nonlinear regression model in GraphPad Prism (version 6.0; Dotmatics, MA, USA), and half maximal inhibitory concentration values are presented as mean ± standard deviation.

Cell Viability Assay

Cell viability was determined using the CellTiter-Glo Luminescent Cell Viability Assay (Promega Corporation, Madison, WI, USA; Cat. No. G7570), which quantifies intracellular adenosine triphosphate as an indicator of metabolically active cells.

Caki-1 cells (ATCC, Manassas, VA, USA; Cat. No. HTB-46) and HK-2 cells (ATCC, Manassas, VA, USA; Cat. No. CRL-2190) were cultured in their respective recommended media under standard conditions (37 °C, 5% carbon dioxide). Cells were seeded in white opaque 96-well plates (Corning Costar, Tewksbury, MA, USA; Cat. No. 3917) at a density of 8×10^3 cells per well and allowed to adhere overnight. Cells were subsequently exposed to HFS764 at concentrations of 0.1, 1, 3, 10, 30 and 100 µM for 72 hours, with a final dimethyl sulfoxide concentration of 0.1% (v/v). Vehicle-treated wells (0.1% dimethyl sulfoxide) and untreated controls were included. Each condition was performed in technical triplicate. All cell lines used in this study were authenticated by short tandem repeat (STR) profiling and were confirmed to be free of mycoplasma contamination prior to experimentation.

At the end of the treatment period, an equal volume of CellTiter-Glo reagent (Promega Corporation, Madison, WI, USA; Cat. No. G7570) was added to each well according to the manufacturer's protocol. Plates were incubated for 10 minutes at room temperature with orbital shaking to ensure complete cell lysis and stabilization of the luminescent sig-

nal. Luminescence was measured using a FLUOstar Omega microplate reader (BMG Labtech, Ortenberg, Germany).

Cell viability was expressed as a percentage relative to vehicle-treated controls. Dose–response relationships were modeled using a four-parameter logistic nonlinear regression analysis in GraphPad Prism (version 6.0). The therapeutic index was calculated as the ratio of half maximal inhibitory concentration values in HK-2 cells to those in Caki-1 cells:

Therapeutic Index (TI) = IC_{50} (HK-2) / IC_{50} (Caki-1)

VEGF Secretion Assay

Secreted VEGF levels were quantified using a human VEGF-A enzyme-linked immunosorbent assay kit (R&D Systems, Quantikine, Cat. No. DVE00) according to the manufacturer's instructions. Caki-1 cells (ATCC, Manassas, VA, USA; Cat. No. HTB-46) were seeded in 24-well plates (Corning Costar, Tewksbury, MA, USA; Cat. No. 3524) at a density of 1.5×10^5 cells per well and allowed to adhere overnight in complete McCoy's 5A medium supplemented with 10% fetal bovine serum and 1% penicillin–streptomycin at 37 °C in a humidified atmosphere containing 5% carbon dioxide.

On the following day, cells were washed once with phosphate-buffered saline and incubated in serum-reduced medium (1% fetal bovine serum, Gibco, Grand Island, NY, USA; Cat. No FBS 10500-064) to minimize baseline growth factor contribution. Cells were then treated with HFS764 at concentrations of 0.1, 1, 3, and 10 µM (final dimethyl sulfoxide concentration 0.1% v/v) or vehicle control (0.1% dimethyl sulfoxide) and subjected to hypoxic conditions (1% oxygen, 5% carbon dioxide, balance nitrogen) for 24 hours using a tri-gas incubator (Galaxy 48 R, Eppendorf, Enfield, CT, USA). Normoxic controls (21% oxygen) were maintained in parallel.

Following treatment, conditioned media were collected and centrifuged at 1000 ×g for 5 minutes to remove cellular debris. Supernatants were stored at –80 °C until analysis. VEGF-A concentrations were determined by enzyme-linked immunosorbent assay using a standard curve generated with recombinant human VEGF-A standards supplied in the kit. Absorbance was measured at 450 nm with wavelength correction at 570 nm using a FLUOstar Omega microplate reader (BMG Labtech, Ortenberg, Germany).

VEGF secretion was expressed as picograms per milliliter and normalized to total viable cell number determined in parallel wells using the CellTiter-Glo assay to account for variations in cell density. Each condition was evaluated in technical triplicate, and experiments were independently repeated three times.

Statistical Analysis

Normality of datasets was assessed using the Shapiro–Wilk test, and homogeneity of variance was evaluated using the Brown–Forsythe test where appropriate prior to conducting parametric analyses. All experiments were performed using at least three independent biological replicates. Data are presented as mean ± standard deviation (SD). Statistical analyses were performed using GraphPad Prism (version 6.0). Comparisons among multiple groups were conducted using one-way analysis of variance (ANOVA), followed by Dunnett's post hoc test for comparisons against control groups. For pairwise comparisons, an unpaired two-tailed Student's *t*-test was applied where appropriate. Concentration–response curves were fitted using a four-parameter logistic (4PL) nonlinear regression model to determine IC_{50} and GI_{50} values. A p-value < 0.05 was considered statistically significant.

Results

Computational Identification of a Druggable Pocket in HIF-1α

To identify potential ligand-binding regions within HIF-1α, a computational structural model was generated and subjected to cavity analysis. The predicted three-dimensional structure displayed a predominantly α-helical organization with clearly defined secondary structural elements (Fig. 1a). Structural evaluation combined with computational pocket detection algorithms revealed a discrete cavity within the within the PAS domain (residues 228–298) of HIF-1α. This cavity, visualized as a green meshed surface embedded within a helical–loop framework, exhibited geometric and spatial characteristics compatible with small-molecule accommodation (Fig. 1b).

To assess the functional relevance of this pocket, a high-throughput virtual screening campaign was performed using a natural product-like subset of the ZINC database. Molecular docking simulations generated a distribution of predicted binding affinities across approximately 250,000 screened compounds (Fig. 1c). Compounds were ranked according to docking score, and candidates located within the high-affinity region of the distribution curve were selected for further structural refinement and experimental validation.

Lead Compound Selection and Interaction Profiling

The top-ranked compounds identified from virtual screening—HFS765, HFS764, HFS766, and HFS767—were further evaluated based on predicted docking energies and binding orientation within the identified pocket (Fig. 1d). These candidates demonstrated consistently lower predicted binding free energies compared with the broader screened library, supporting their prioritization for detailed interaction analysis.

Analysis of the docking-derived binding modes revealed that all four compounds occupied a similar region within the cavity spanning residues 776–826 of HIF-1α. Protein–ligand interaction profiling indicated stabi-

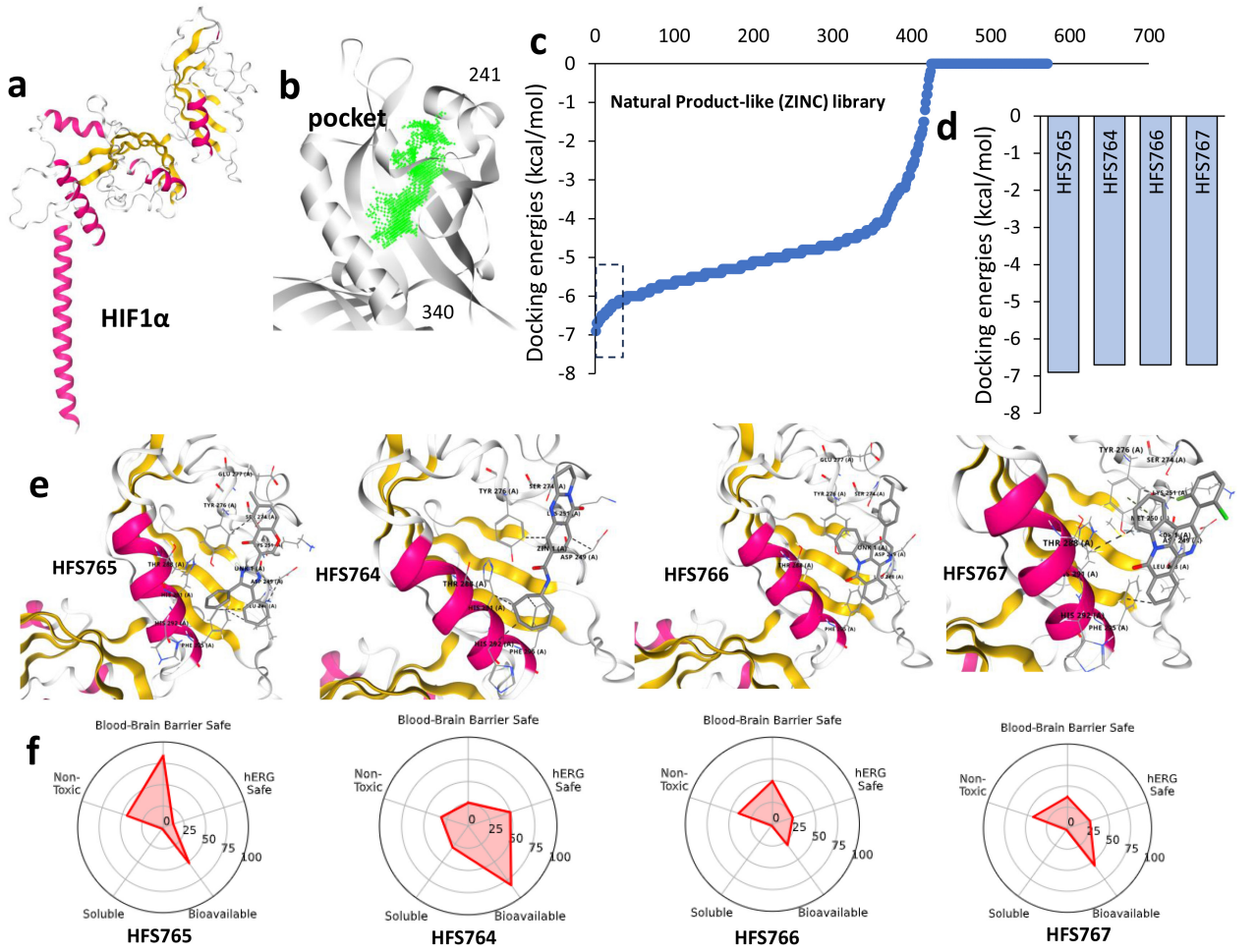

Fig. 1. High-throughput structure-based virtual screening targeting HIF-1α. (a) Three-dimensional structural model of HIF-1α obtained from the AlphaFold database. (b) Predicted ligand-binding pocket located within the PAS domain (residues 228–298), shown as a green mesh representation. (c) High-throughput virtual screening of a natural product-like subset from the ZINC database, with compounds ranked according to docking scores. (d) Predicted docking scores of the top lead compounds against HIF-1α. (e) Protein–ligand interaction analysis of the selected lead compounds within the identified binding pocket, highlighting interacting HIF-1α residues. (f) *In silico* ADMET property assessment of the prioritized lead compounds. HIF-1α, hypoxia-inducible factor-1 alpha; ZINC, ZINC000002051026; ADMET, absorption, distribution, metabolism, excretion, and toxicity.

lization through a combination of hydrogen bonding and hydrophobic contacts, involving residues such as threonine, histidine, tyrosine, aspartate, and phenylalanine lining the pocket (Fig. 1e). These interactions reflect geometric and electrostatic complementarity between the ligands and the binding cavity, supporting stable accommodation within the helical–loop framework of the C-terminal region. Among the evaluated candidates, HFS764 exhibited a well-balanced interaction profile, with consistent hydrogen bonding and hydrophobic interactions, supporting its selection for subsequent biochemical and functional validation.

In Silico ADMET Profiling and Lead Prioritization

To further prioritize lead candidates, in silico absorption, distribution, metabolism, excretion, and toxicity (ADMET) profiling was performed. The prioritized compounds, including HFS764, demonstrated physicochemical properties consistent with drug-like characteristics, including acceptable aqueous solubility and predicted oral absorption (Fig. 1f). Safety-related predictions indicated low blood–brain barrier permeability, which may reduce the risk of central nervous system–associated effects. Evaluation of metabolic liabilities suggested minimal predicted inhibition of major cytochrome P450 isoforms, indicating a lower potential for drug–drug interactions. In addition, toxicity prediction models did not indicate significant risks of mutagenicity or hepatotoxicity.

Integration of docking performance with ADMET characteristics supported prioritization of HFS764 as the most balanced candidate. HFS764 combined stable predicted binding within the identified HIF-1α cavity with fa-

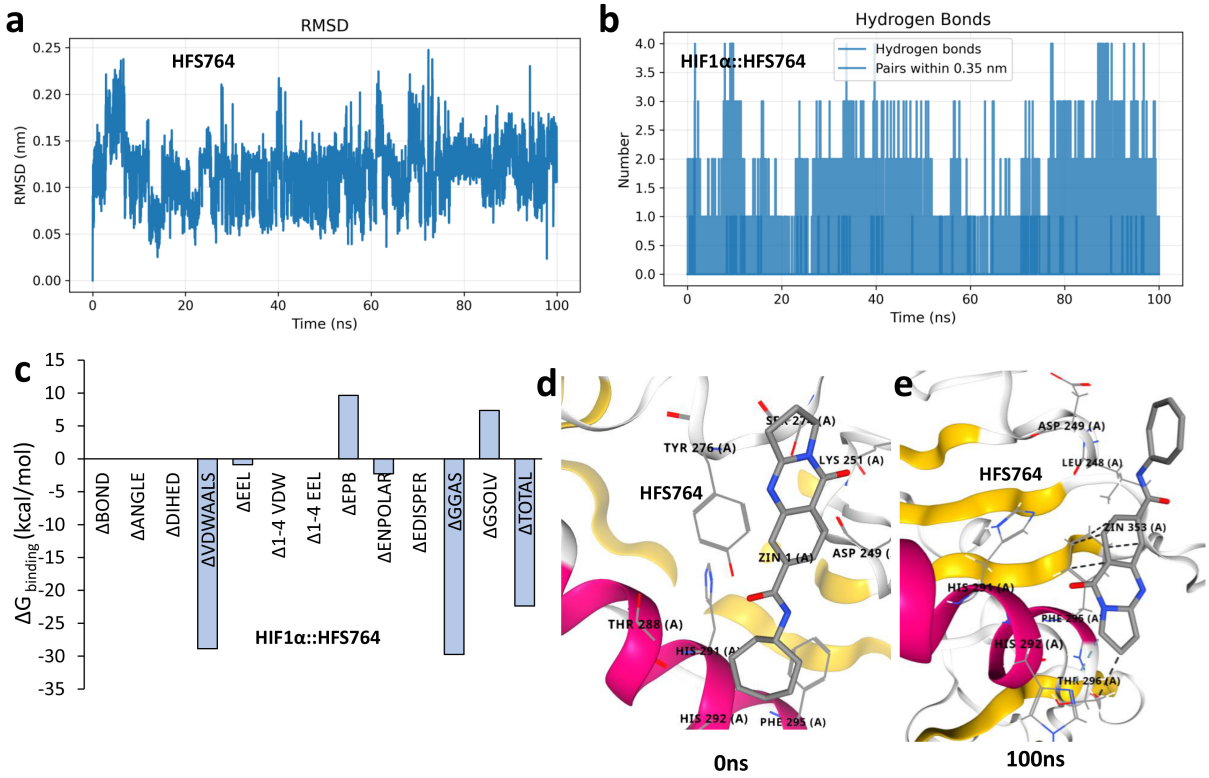

Fig. 2. Molecular dynamics simulation of the HIF-1α–HFS764 complex. (a) Ligand root-mean-square deviation (RMSD) over a 100 ns simulation trajectory for the HIF-1α–HFS764 complex. (b) Time-resolved analysis of intermolecular interactions between HFS764 and HIF-1α during the 100 ns trajectory. (c) Estimated binding free energy derived from the molecular dynamics simulation. (d) Structural snapshot of the initial docking pose prior to simulation. (e) Structural snapshot of the complex after 100 ns of molecular dynamics simulation.

vorable pharmacokinetic and safety parameters, supporting its advancement for biochemical and cellular validation. A two-dimensional interaction schematic illustrating the predicted binding orientation of HFS764 within the HIF-1α pocket is provided in **Supplementary Fig. 1**.

Molecular Dynamics and Binding Energetics of HFS764 With HIF-1α

To assess the conformational stability of the HIF-1α–HFS764 complex, a 100-ns molecular dynamics simulation was conducted. Analysis of ligand root-mean-square deviation (RMSD) across the trajectory demonstrated fluctuations predominantly below 0.20 nm, indicating minimal positional drift and stable retention of HFS764 within the binding cavity throughout the simulation period (Fig. 2a).

Intermolecular interaction analysis further revealed sustained hydrogen bond formation between HFS764 and residues lining the binding pocket. These interactions persisted over the course of the simulation, supporting maintenance of a stable protein–ligand contact network (Fig. 2b).

Binding energetics were estimated through energy decomposition analysis of the simulation trajectory. The calculated total binding free energy (ΔG_total) of –22.38 kcal/mol indicated favorable intermolecular affinity, with substantial contributions from both van der Waals interactions and electrostatic forces (Fig. 2c). The combined energetic profile The calculated binding free energy (ΔG_total) of –22.38 kcal/mol indicated favorable intermolecular affinity, with contributions from both van der Waals and electrostatic interactions (Fig. 2c). Analysis of the simulation trajectory revealed that hydrophobic stabilization was primarily driven by persistent contacts between HFS764 and nonpolar residues lining the binding cavity, including Leu248 and Phe295, which facilitate favorable van der Waals interactions and promote ligand retention within the pocket. In parallel, polar interactions contributed to binding specificity, as evidenced by sustained hydrogen bonding and electrostatic contacts with residues such as Asp249, His291, and His292. These interactions were maintained for a significant portion of the simulation trajectory, indicating stable ligand engagement.

Together, the combined persistence of hydrophobic contacts and polar interactions across the trajectory supports a cooperative stabilization mechanism, in which hy-

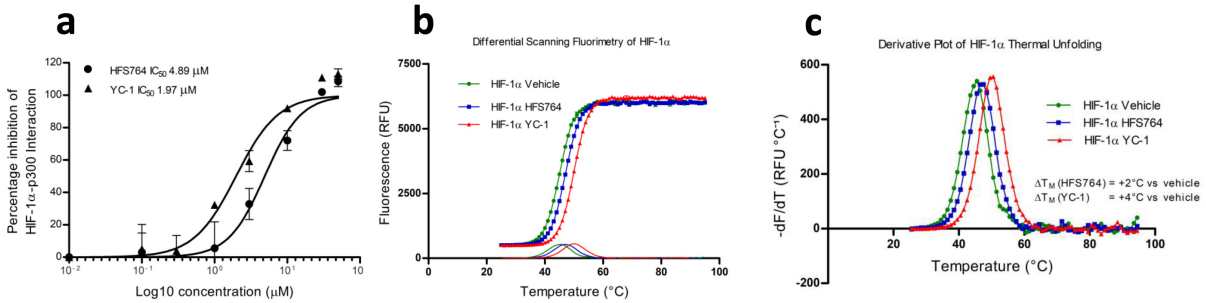

Fig. 3. Biochemical and biophysical validation of HFS764 interaction with HIF-1α. (a) HTRF concentration–response curves showing concentration-dependent reduction of the HIF-1α–p300 interaction-associated HTRF signal by HFS764 and the reference inhibitor YC-1. Data are presented as mean ± SD from three independent experiments, each performed in technical triplicate. Nonlinear regression analysis yielded IC_{50} values of 4.89 µM for HFS764 and 1.97 µM for YC-1. (b) Differential scanning fluorimetry (DSF) melt curves of recombinant HIF-1α C-TAD (residues 776–826) in the presence of HFS764 (50 µM), YC-1 (50 µM), or vehicle control (1% DMSO). Both compounds produced rightward shifts in thermal unfolding profiles relative to vehicle, consistent with ligand-induced stabilization. (c) First-derivative plots (–dF/dT) used to determine melting temperatures (T_m). Vehicle-treated HIF-1α exhibited a T_m of 47.5 °C, whereas HFS764 and YC-1 increased T_m to 49.5 °C (ΔT_m = +2.0 °C) and 51.5 °C (ΔT_m = +4.0 °C), respectively. Data represent mean values obtained from replicate measurements across independent assay runs. Underlying numerical source data corresponding to these analyses are provided in **Supplementary Source Data 1**. HTRF, homogeneous time-resolved fluorescence; SD, standard deviation; C-TAD, C-terminal transactivation domain; DMSO, dimethyl sulfoxide.

drophobic packing anchors the ligand within the cavity while polar interactions contribute to orientation and specificity of binding.

Structural comparison between the initial docking pose and the post-simulation conformation demonstrated preservation of the overall binding orientation. In the pre-simulation structure, HFS764 formed contacts with residues including Thr288, His291, His292, Tyr276, Lys251, Asp249, and Phe295 (Fig. 2d). After 100 ns of simulation, the ligand remained embedded within the cavity and retained proximity to Asp249, Leu248, His291, His292, Phe295, and Thr296 (Fig. 2e), confirming positional stability and conservation of key interaction networks.

HTRF Biochemical Assay

To evaluate whether HFS764 functionally interferes with the interaction between HIF-1α and its transcriptional coactivator p300, a cell-free homogeneous time-resolved fluorescence binding assay was performed using recombinant HIF-1α C-terminal transactivation domain (C-TAD) and the p300 CH1 domain. Treatment with HFS764 resulted in a concentration-dependent reduction in fluorescence resonance energy transfer signal, consistent with inhibition of HIF-1α–p300 complex formation (Fig. 3a). Nonlinear regression analysis of the concentration–response curve yielded a half maximal inhibitory concentration (IC_{50}) of 4.89 µM. The selected concentration range (0.01–50 µM) adequately captured the full dynamic response of the assay, encompassing both subthreshold and saturating inhibition consistent with the observed IC_{50} values.

For assay benchmarking, the reference HIF pathway inhibitor YC-1 was evaluated under identical conditions. YC-1 exhibited a more potent inhibitory profile, with an IC_{50} of 1.97 µM, consistent with the reported low micromolar activity of YC-1 in HIF-related biochemical and transcriptional assays [12,13,14]. The observed difference in potency between YC-1 and HFS764 confirms the dynamic range and sensitivity of the assay while demonstrating measurable inhibitory activity of HFS764 within the low µM range. It is important to note that YC-1 is not a direct inhibitor of the HIF-1α–p300 interface but acts upstream by modulating HIF-1α stability and transcriptional activity. The observed inhibitory signal in this assay therefore reflects its functional impact on HIF-related pathways rather than specific disruption of the protein–protein interaction.

Collectively, these findings support functional interference of HFS764 with the HIF-1α–p300 interaction in a concentration-dependent manner and are consistent with the computationally predicted binding mode identified through virtual screening. Numerical source data underlying Fig. 3 biochemical and biophysical assays are provided as **Supplementary Source Data 1**.

Differential Scanning Fluorimetry Confirms Ligand-Induced Thermal Stabilization

Differential scanning fluorimetry was performed to assess thermal stabilization of the HIF-1α C-terminal transactivation domain (C-TAD) in the presence of HFS764. Relative to vehicle-treated protein, HFS764 produced a rightward shift in the thermal unfolding profile, consistent with ligand-induced stabilization (Fig. 3b). Derivative analysis of the unfolding curves indicated a melting temper-

ature (T_m) of 47.5 °C for vehicle-treated HIF-1α, whereas incubation with HFS764 increased the T_m to 49.5 °C, corresponding to a thermal shift (ΔT_m) of +2.0 °C (Fig. 3c). The reference inhibitor YC-1 produced a larger stabilization effect, increasing the HIF-1α melting temperature to 51.5 °C (ΔT_m = +4.0 °C relative to vehicle). The corresponding melt curves and first-derivative plots are provided in **Supplementary Fig. 2**. The magnitude and direction of the observed thermal shifts are consistent with ligand-induced stabilization of the HIF-1α C-TAD domain. These biophysical findings align with the HTRF assay results and further support interaction of HFS764 with the targeted HIF-1α C-TAD region.

HFS764 Inhibits HIF-1 Transcriptional Activity Under Hypoxia and Metabolic Stress

To assess functional activity in a cellular context, HIF-1 transcriptional activity was quantified using a hypoxia response element (HRE)-driven dual-luciferase reporter assay in Caki-1 cells subjected to combined metabolic stress and hypoxia. Cells were cultured under high-glucose conditions (25 mM) together with 1% oxygen to model a metabolically stressed environment known to potentiate HIF-1α signaling and approximate tumor-associated stress conditions *in vivo*. Under these conditions, treatment with HFS764 resulted in a concentration-dependent reduction of hypoxia-induced HRE reporter activity across the 0.01–30 µM range (Fig. 4a). Nonlinear regression analysis yielded a half maximal inhibitory concentration (IC_{50}) of 4.27 µM. The reference inhibitor YC-1 similarly inhibited HRE-driven transcription under identical conditions, with an IC_{50} of 3.47 µM (Fig. 4a), consistent with the reported low micromolar inhibitory activity of YC-1 in HIF-dependent transcriptional assays [12,13,14] (Fig. 4a). At higher concentrations, both compounds markedly reduced reporter activity, demonstrating preserved assay sensitivity and confirming low-µM inhibitory activity of HFS764 in a cellular setting.

These findings indicate that HFS764 attenuates HIF-1–dependent transcriptional activity under integrated hypoxic and metabolic stress conditions, extending the biochemical inhibition observed in cell-free assays to a functional cellular context.

Cell Viability and Selectivity of HFS764 in ccRCC Versus Normal Renal Epithelial Cells

To determine whether suppression of HIF-1 transcriptional activity was associated with altered cellular proliferation, the cytotoxic profile of HFS764 was evaluated using a CellTiter-Glo luminescence assay following 72-hour exposure in Caki-1 renal carcinoma cells and non-tumorigenic HK-2 renal epithelial cells. Treatment with HFS764 produced a concentration-dependent reduction in Caki-1 cell viability across the tested range (0.1–100 µM), with a fitted half maximal growth inhibitory concentration (GI_{50}) of 14.70 µM determined by four-parameter nonlinear regression analysis (Fig. 4b).

In contrast, HK-2 cells exhibited a right-shifted dose–response curve, with a GI_{50} of 37.98 µM under identical experimental conditions (Fig. 4b). At concentrations ≤10 µM, HK-2 cell viability remained at or above 80%, whereas Caki-1 cells demonstrated greater sensitivity within the same concentration range, indicating differential responsiveness between malignant and non-malignant renal cells.

The therapeutic index (TI), calculated as the ratio of GI_{50} in HK-2 cells to GI_{50} in Caki-1 cells, was 2.58 (37.98/14.70), reflecting approximately 2.6-fold selectivity *in vitro*. The GI_{50} observed in Caki-1 cells occurred at concentrations modestly higher than the HRE-luciferase IC_{50} (~4 µM), consistent with a model in which transcriptional inhibition precedes measurable effects on cell viability.

Collectively, these findings indicate that HFS764 reduces ccRCC cell viability in a concentration-dependent manner while exhibiting comparatively lower cytotoxicity in non-malignant renal epithelial cells, supporting further evaluation of HFS764 as a selective modulator of HIF-1 signaling.

HFS764 Suppresses Hypoxia-Induced VEGF Secretion in Caki-1 Cells

To evaluate whether inhibition of HIF-1 transcriptional activity was associated with reduced angiogenic signaling, vascular endothelial growth factor (VEGF) secretion was quantified in conditioned media from hypoxia-exposed Caki-1 cells. Exposure to 1% oxygen for 24 hours significantly increased VEGF secretion compared with normoxic controls, confirming activation of the hypoxia-responsive pathway.

Treatment with HFS764 produced a concentration-dependent decrease in hypoxia-induced VEGF secretion (Fig. 5). At 0.1 µM, VEGF levels were reduced relative to hypoxia plus vehicle-treated controls. Increasing concentrations (1–10 µM) resulted in progressively greater suppression, with the highest concentration substantially reducing VEGF secretion toward normoxic baseline levels.

These data indicate that inhibition of HIF-1 signaling by HFS764 translates into attenuation of downstream pro-angiogenic output under hypoxic conditions. The observed reduction in VEGF secretion is consistent with suppression of HRE-driven transcriptional activity and supports the mechanistic link between HIF-1 pathway inhibition and impaired angiogenic signaling in Caki-1 cells.

Discussion

In this study, we employed an integrated structure-guided and experimental approach to identify HFS764 as a novel small-molecule inhibitor targeting the HIF-1α transcriptional machinery. Computational modeling re-

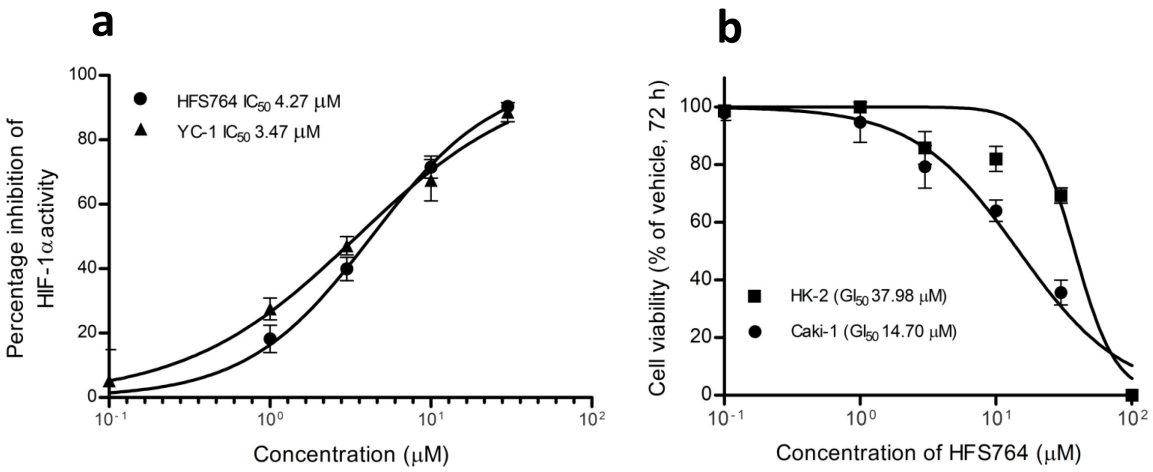

Fig. 4. HFS764 suppresses HIF-1 transcriptional activity and reduces ccRCC cell viability with measurable selectivity. (a) HFS764 inhibits hypoxia-induced HIF-1–dependent transcriptional activity in Caki-1 cells. Cells were co-transfected with a 5×HRE firefly luciferase reporter construct and a Renilla luciferase normalization vector, followed by exposure to hypoxia (1% O_2) for 18 h in the presence of increasing concentrations of HFS764 (0.01–30 μM) or the reference inhibitor YC-1. Firefly luciferase activity was normalized to Renilla luciferase and expressed as percent inhibition relative to hypoxia plus vehicle controls. Nonlinear regression analysis using a four-parameter logistic model yielded IC_{50} values of 4.27 μM for HFS764 and 3.47 μM for YC-1. (b) HFS764 reduces ccRCC cell viability with limited cytotoxicity toward non-malignant renal epithelial cells. Caki-1 and HK-2 cells were treated with HFS764 (0.1–100 μM) for 72 h, and cell viability was quantified using the CellTiter-Glo® luminescence assay. Viability was expressed as a percentage of vehicle-treated controls. Dose–response curves were fitted using a four-parameter logistic model to determine GI_{50} values of 14.70 μM for Caki-1 and 37.98 μM for HK-2 cells. The calculated therapeutic index (GI_{50} HK-2/GI_{50} Caki-1) was 2.58, indicating preferential sensitivity of tumor cells. Data are presented as mean ± SD from three independent biological experiments, each conducted in technical triplicate. ccRCC, clear cell renal cell carcinoma; HRE, hypoxia response element.

vealed a druggable cavity within the HIF-1α C-terminal transactivation domain, and molecular dynamics simulations supported stable ligand engagement. Biochemical validation demonstrated concentration-dependent suppression of the HIF-1α–p300 interaction-associated signal with low-micromolar potency in hypoxic Caki-1 cells, HFS764 suppressed HIF-dependent transcriptional activity, and reduced VEGF secretion in a concentration-dependent manner. Collectively, these findings establish a mechanistic link between direct interference with the HIF-1α transcriptional interface and downstream attenuation of hypoxia-driven oncogenic signaling, supporting HFS764 as a promising lead for targeting hypoxic RCC.

HIF-1α coordinates adaptive transcriptional responses to hypoxia by activating gene networks that promote angiogenesis, metabolic reprogramming, and tumor cell survival in ccRCC [5]. Central to this response is the interaction between the HIF-1α C-TAD and the CH1 domain of p300/CBP [15,16]. Disruption of this protein–protein interface represents a rational strategy to attenuate HIF-1–dependent transcription and downstream oncogenic signaling [15,16]. Using a structure-guided computational workflow, we identified a cavity within the HIF-1α PAS domain (residues 228–298) compatible with small-molecule binding. Virtual screening enriched compounds with favorable predicted interactions, and HFS764 emerged based on docking performance and interaction profiling. These findings are consistent with prior structural studies demonstrating that HIF-1α C-TAD adopts a more ordered conformation upon p300 binding, stabilized through hydrophobic and polar interactions [17,18].

MD simulations provided dynamic validation of the docking model. Across a 100-ns trajectory, HFS764 remained confined within the predicted pocket with low RMSD fluctuation and persistent hydrogen bond formation. Binding free energy estimation revealed favorable contributions from van der Waals and electrostatic interactions, supporting a thermodynamically plausible mode of stabilization. Structural comparison of pre- and post-MD conformations confirmed retention of key ligand–protein contacts.

Biochemical validation using an HTRF assay demonstrated concentration-dependent suppression of the HIF-1α–p300 interaction-associated signal with low-μM potency. In Caki-1 cells subjected to combined hypoxia and metabolic stress, HFS764 suppressed HRE-driven transcriptional activity within a comparable concentration range. Inclusion of high glucose in the reporter assay reflects metabolic stress known to potentiate HIF-1α signaling [7,19] whereas downstream assays under hypoxia

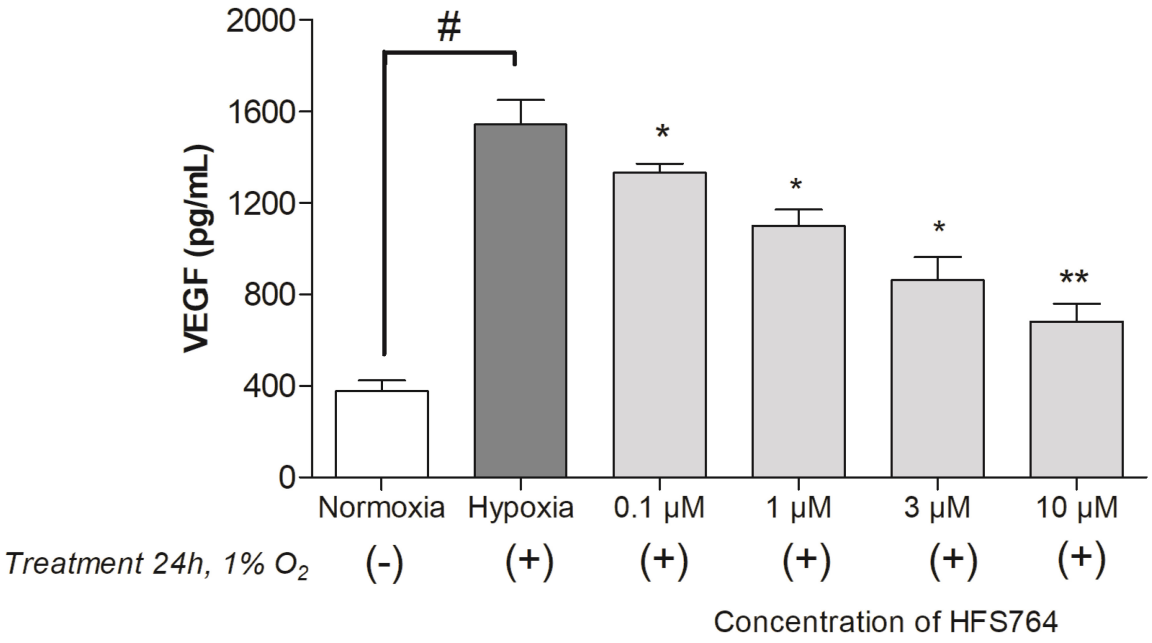

Fig. 5. HFS764 suppresses VEGF secretion in hypoxic Caki-1 cells. VEGF levels were quantified in conditioned media from Caki-1 cells exposed to normoxia or hypoxia (1% O_2) for 24 h in the presence of increasing concentrations of HFS764 (0.1–10 μM). Hypoxia significantly increased VEGF secretion relative to normoxic controls. HFS764 treatment produced a concentration-dependent reduction in hypoxia-induced VEGF levels. Data are presented as mean ± SD from three independent biological experiments, each performed in technical triplicate. Statistical analysis was performed using one-way ANOVA followed by Dunnett's multiple comparisons test. $^{\#}p < 0.05$ versus normoxic control; $^{*}p < 0.05$ and $^{**}p < 0.01$ versus hypoxia + vehicle.

alone allowed evaluation of canonical HIF-mediated phenotypes. Differential scanning fluorimetry showed ligand-induced stabilization of the HIF-1α C-terminal domain, consistent with ligand-induced stabilization suggestive of protein–ligand interaction. However, DSF provides indirect evidence and does not alone confirm binding. Therefore, these results were interpreted alongside orthogonal findings. These findings include a concentration-dependent reduction in the HIF-1α–p300 interaction-associated HTRF signal, together with stable ligand retention observed during molecular dynamics simulations, collectively supporting the interaction of HFS764 with HIF-1α. YC-1 was used in this study as a functional comparator rather than as a direct inhibitor of the HIF-1α–p300 coactivator interface. Unlike YC-1, HFS764 was computationally prioritized based on its predicted interaction with the HIF-1α transcriptional coactivator interface, whereas YC-1 primarily modulates HIF-1α stability and signaling through upstream mechanisms. This distinction highlights the mechanistic relevance of HFS764 as a direct modulator of the transcriptional complex and suggests a more targeted strategy compared with indirect modulation of the HIF signaling pathway.

Several small-molecule inhibitors targeting the HIF-1α C-TAD–p300 interaction have been reported, providing important context for evaluating the activity of HFS764. Structural studies have established that the HIF-1α C-terminal transactivation domain adopts a defined conformation upon binding to the p300 CH1 domain, forming a critical interface required for transcriptional activation [20,21]. Early pharmacological disruption of this interaction was achieved using chetomin, which inhibits HIF-1α–p300 binding through zinc ejection from the p300 CH1 domain. However, chetomin is associated with significant cytotoxicity and limited selectivity, constraining its translational potential. Subsequent efforts identified small molecules such as KCN1 that inhibit HIF-1α–p300 interaction and suppress tumor growth, although these compounds often exhibit moderate potency and variable pharmacological profiles [22,23].

In this context, HFS764 represents a structure-guided approach targeting a defined cavity within the HIF-1α C-TAD, supported by integrated computational, biochemical, and cellular validation. Unlike indirect modulators such as YC-1 or zinc-disrupting agents such as chetomin, HFS764 was identified through a structure-based workflow designed to target the transcriptional interface and demonstrated consistent activity across computational, biochemical, and cellular platforms. The observed low-micromolar inhibition of the HIF-1α–p300 interaction, together with consistent suppression of HIF-dependent transcription and downstream VEGF signaling, supports its functional rele-

vance. Importantly, the convergence of structural modeling, biophysical stabilization, and functional cellular activity distinguishes HFS764 from earlier inhibitors that often lacked multi-level validation.

Hypoxia-induced VEGF upregulation is a principal driver of tumor angiogenesis [24,25]. In hypoxic Caki-1 cells, VEGF secretion increased relative to normoxic conditions, consistent with activation of HIF-dependent transcriptional programs. Treatment with HFS764 reduced hypoxia-induced VEGF secretion in a concentration-dependent manner, indicating that disruption of HIF-1–mediated transcription translates into attenuation of downstream pro-angiogenic signaling. Similar reductions in VEGF expression following pharmacological or genetic inhibition of HIF signaling have been described in hypoxic tumor models, supporting the functional linkage between HIF pathway suppression and impaired angiogenic signaling [26,27].

Collectively, these findings support a mechanistic framework in which HFS764 attenuates hypoxia-driven oncogenic signaling through disruption of the HIF-1α transcriptional interface, resulting in reduced VEGF secretion.

Future investigations should include *in vivo* pharmacodynamic and antitumor efficacy studies, comprehensive pharmacokinetic (PK) characterization, and assessment of tissue distribution profiles. Evaluation of combination strategies with established targeted therapies or immunotherapeutic agents may further define therapeutic applicability. In addition, systematic structure–activity relationship (SAR) optimization could enhance potency and target selectivity, thereby facilitating translational development of HFS764.

Despite the integrated computational, biochemical, and cellular evidence supporting HFS764 as a modulator of HIF-1α–dependent transcriptional signaling, several limitations warrant consideration. Functional validation was conducted using a single renal carcinoma model (Caki-1). Although this model is well established for studying hypoxia-driven HIF signaling, reliance on a single cell line may limit the broader applicability of these findings given the molecular heterogeneity of ccRCC. Evaluation across additional ccRCC cell lines, particularly those with distinct genetic backgrounds such as differences in VHL status, would further enhance the robustness and translational relevance of the observed effects.

Although inhibition of VEGF secretion is consistent with downstream consequences of HIF inhibition, broader profiling of additional HIF-regulated target genes and associated signaling pathways would further define the mechanistic scope of HFS764 activity. Moreover, *in vivo* pharmacodynamic and antitumor efficacy studies are necessary to establish translational relevance, including evaluation of bioavailability, tissue distribution, pharmacokinetic properties, and systemic safety. These limitations identify important areas for future investigation but do not diminish the integrated mechanistic evidence supporting disruption of hypoxia-driven HIF signaling by HFS764.

Additional orthogonal biophysical and biochemical approaches, including surface plasmon resonance, microscale thermophoresis, isothermal titration calorimetry, and co-immunoprecipitation assays, would further substantiate the mechanistic characterization of HFS764 interaction with the HIF-1α–p300 complex.

Conclusion

This study identifies HFS764 as a small-molecule inhibitor targeting hypoxia-driven HIF signaling through functional disruption of HIF-1α–dependent transcriptional activity associated with the HIF-1α–p300 interface. Integrated computational modeling, biochemical validation, and functional cellular analyses collectively demonstrate that HFS764 suppresses HIF-dependent transcriptional activity, reduces VEGF secretion in hypoxic Caki-1 renal carcinoma cells. The observed transition from computationally predicted interface engagement to attenuation of angiogenic signaling provides mechanistic support for the therapeutic potential of targeting transcriptional coactivator interactions in hypoxic malignancies. Collectively, these findings establish HFS764 as a lead compound that warrants further pharmacological optimization and preclinical evaluation in HIF-driven cancers.

Availability of Data and Materials

All data generated or analyzed during this study are included in this published article. Additional information are available from the corresponding author upon reasonable request for academic research purposes.

Author Contributions

MMAS is the sole contributor to this manuscript. The author confirms sole responsibility for the conception and design of the study; the acquisition, analysis, and interpretation of data; the preparation of the manuscript; reading and approving the final manuscript; and for being accountable for all aspects of the work.

Ethics Approval and Consent to Participate

Not applicable.

Acknowledgment

Not applicable.

Funding

This work was supported by the Deanship of Scientific Research, King Khalid University, Saudi Arabia, under the Small Research Groups funding program (Grant No. RGP.1/193/46).

Conflict of Interest

The author declares no conflict of interest.

Supplementary Material

Supplementary material associated with this article can be found, in the online version, at https://doi.org/10.24976/Discov.Med.202638211.200.

References

[1] Kelly JF, Samarska IV, Ramaekers B, Marcelissen T, van Roermund JG, Aarts MJB, et al. Renal cell carcinoma detection: a systematic review in diagnostic urinary biomarkers. BMC Cancer. 2025; 25: 1672. https://doi.org/10.1186/s12885-025-14900-8

[2] Dong Z, Li S, Li M, Fan M, Chen K, Li A, et al. Recent progress on tyrosine kinase inhibitors resistance in renal cell carcinoma: another brick in the wall? Cancer Drug Resistance (Alhambra, Calif.). 2025; 8: 54. https://doi.org/10.20517/cdr.2025.157

[3] Schödel J, Grampp S, Maher ER, Moch H, Ratcliffe PJ, Russo P, et al. Hypoxia, Hypoxia-inducible Transcription Factors, and Renal Cancer. European Urology. 2016; 69: 646–657. https://doi.org/10.1016/j.eururo.2015.08.007

[4] Mazumder S, Higgins PJ, Samarakoon R. Downstream Targets of VHL/HIF-α Signaling in Renal Clear Cell Carcinoma Progression: Mechanisms and Therapeutic Relevance. Cancers. 2023; 15: 1316. https://doi.org/10.3390/cancers15041316

[5] Basheeruddin M, Qausain S. Hypoxia-Inducible Factor 1-Alpha (HIF-1α) and Cancer: Mechanisms of Tumor Hypoxia and Therapeutic Targeting. Cureus. 2024; 16: e70700. https://doi.org/10.7759/cureus.70700

[6] Zhao Y, Xing C, Deng Y, Ye C, Peng H. HIF-1α signaling: Essential roles in tumorigenesis and implications in targeted therapies. Genes & Diseases. 2023; 11: 234–251. https://doi.org/10.1016/j.gendis.2023.02.039

[7] Iacobini C, Vitale M, Pugliese G, Menini S. Normalizing HIF-1α Signaling Improves Cellular Glucose Metabolism and Blocks the Pathological Pathways of Hyperglycemic Damage. Biomedicines. 2021; 9: 1139. https://doi.org/10.3390/biomedicines9091139

[8] Gunton JE. Hypoxia-inducible factors and diabetes. The Journal of Clinical Investigation. 2020; 130: 5063–5073. https://doi.org/10.1172/JCI137556

[9] Yfantis A, Mylonis I, Chachami G, Nikolaidis M, Amoutzias GD, Paraskeva E, et al. Transcriptional Response to Hypoxia: The Role of HIF-1-Associated Co-Regulators. Cells. 2023; 12: 798. https://doi.org/10.3390/cells12050798

[10] Qin X, Chen H, Tu L, Ma Y, Liu N, Zhang H, et al. Potent Inhibition of HIF1α and p300 Interaction by a Constrained Peptide Derived from CITED2. Journal of Medicinal Chemistry. 2021; 64: 13693–13703. https://doi.org/10.1021/acs.jmedchem.1c01043

[11] Swanson K, Walther P, Leitz J, Mukherjee S, Wu JC, Shivnaraine RV, et al. ADMET-AI: a machine learning ADMET platform for evaluation of large-scale chemical libraries. Bioinformatics (Oxford, England). 2024; 40: btae416. https://doi.org/10.1093/bioinformatics/btae416

[12] Ouyang C, Zhang J, Lei X, Xie Z, Liu X, Li Y, et al. Advances in antitumor research of HIF-1α inhibitor YC-1 and its derivatives. Bioorganic Chemistry. 2023; 133: 106400. https://doi.org/10.1016/j.bioorg.2023.106400

[13] Lau CK, Yang ZF, Lam CT, Tam KH, Poon RTP, Fan ST. Suppression of hypoxia inducible factor-1alpha (HIF-1alpha) by YC-1 is dependent on murine double minute 2 (Mdm2). Biochemical and Biophysical Research Communications. 2006; 348: 1443–1448. https://doi.org/10.1016/j.bbrc.2006.08.015

[14] Li SH, Shin DH, Chun YS, Lee MK, Kim MS, Park JW. A novel mode of action of YC-1 in HIF inhibition: stimulation of FIH-dependent p300 dissociation from HIF-1{alpha}. Molecular Cancer Therapeutics. 2008; 7: 3729–3738. https://doi.org/10.1158/1535-7163.MCT-08-0074

[15] Sun HL, Liu YN, Huang YT, Pan SL, Huang DY, Guh JH, et al. YC-1 inhibits HIF-1 expression in prostate cancer cells: contribution of Akt/NF-kappaB signaling to HIF-1alpha accumulation during hypoxia. Oncogene. 2007; 26: 3941–3951. https://doi.org/10.1038/sj.onc.1210169

[16] Yeo EJ, Chun YS, Cho YS, Kim J, Lee JC, Kim MS, et al. YC-1: a potential anticancer drug targeting hypoxia-inducible factor 1. Journal of the National Cancer Institute. 2003; 95: 516–525. https://doi.org/10.1093/jnci/95.7.516

[17] Freedman SJ, Sun ZYJ, Poy F, Kung AL, Livingston DM, Wagner G, et al. Structural basis for recruitment of CBP/p300 by hypoxia-inducible factor-1 alpha. Proceedings of the National Academy of Sciences of the United States of America. 2002; 99: 5367–5372. https://doi.org/10.1073/pnas.082117899

[18] Zoccola D, Morain J, Pagès G, Caminiti-Segonds N, Giuliano S, Tambutté S, et al. Structural and functional analysis of coral Hypoxia Inducible Factor. PloS One. 2017; 12: e0186262. https://doi.org/10.1371/journal.pone.0186262

[19] Bhattacharya S, Michels CL, Leung MK, Arany ZP, Kung AL, Livingston DM. Functional role of p35srj, a novel p300/CBP binding protein, during transactivation by HIF-1. Genes & Development. 1999; 13: 64–75. https://doi.org/10.1101/gad.13.1.64

[20] Dames SA, Martinez-Yamout M, De Guzman RN, Dyson HJ, Wright PE. Structural basis for Hif-1 alpha /CBP recognition in the cellular hypoxic response. Proceedings of the National Academy of Sciences of the United States of America. 2002; 99: 5271–5276. https://doi.org/10.1073/pnas.082121399

[21] Lum JJ, Bui T, Gruber M, Gordan JD, DeBerardinis RJ, Covello KL, et al. The transcription factor HIF-1alpha plays a critical role in the growth factor-dependent regulation of both aerobic and anaerobic glycolysis. Genes & Development. 2007; 21: 1037–1049. https://doi.org/10.1101/gad.1529107

[22] Hóbor F, Hegedüs Z, Ibarra AA, Petrovicz VL, Bartlett GJ, Sessions RB, et al. Understanding p300-transcription factor interactions using sequence variation and hybridization. RSC Chemical Biology. 2022; 3: 592–603. https://doi.org/10.1039/d2cb00026a

[23] Jiang W, Abdulkadir S, Zhao X, Sang P, Tomatsidou A, Zhang X, et al. Inhibition of Hypoxia-Inducible Transcription Factor (HIF-1α) Signaling with Sulfonyl-γ-AApeptide Helices. Journal of the American Chemical Society. 2023; 145: 20009–20020. https://doi.org/10.1021/jacs.3c06694

[24] Xu R, Wang F, Yang H, Wang Z. Action Sites and Clinical Application of HIF-1α Inhibitors. Molecules (Basel, Switzerland). 2022; 27: 3426. https://doi.org/10.3390/molecules27113426

[25] Yin S, Kaluz S, Devi NS, Jabbar AA, de Noronha RG, Mun J, et al. Arylsulfonamide KCN1 inhibits in vivo glioma growth and interferes with HIF signaling by disrupting HIF-1α interaction with cofactors p300/CBP. Clinical Cancer Research : an Official Journal of the American Association for Cancer Research. 2012; 18: 6623–6633. https://doi.org/10.1158/1078-0432.CCR-12-0861

[26] Obeagu EI. Hypoxia-driven angiogenesis in breast cancer mechanisms and therapeutic targets: a narrative review. Annals of Medicine and Surgery (2012). 2025; 87: 4246–4254. https://doi.org/10.1097/MS9.0000000000003411

[27] Nicolas S, Abdellatef S, Haddad MA, Fakhoury I, El-Sibai M. Hypoxia and EGF Stimulation Regulate VEGF Expression in Human Glioblastoma Multiforme (GBM) Cells by Differential Regulation of the PI3K/Rho-GTPase and MAPK Pathways. Cells. 2019; 8: 1397. https://doi.org/10.3390/cells8111397